Orbital splitting and optical conductivity of the insulating state of NbO_2

Franklin J. Wong,[1] Nina Hong,[2] and Shriram Ramanathan[1]
[1]*School of Engineering and Applied Sciences, Harvard University, Cambridge, Massachusetts 02138, USA*
[2]*J. A. Woollam Co., Inc, Lincoln, Nebraska 68508, USA*
(Received 27 June 2014; revised manuscript received 24 August 2014; published 22 September 2014)

Optical properties from 0.2 to 6.5 eV of epitaxial NbO_2 ($4d^1$ system) films in their insulating states have been investigated by spectroscopic ellipsometry. The optical spectra are compared to that of epitaxial VO_2 ($3d^1$ system) in its insulating phase. Both compounds are insulators at room temperature and undergo temperature-induced metal-insulator transitions. We find a $d_{||}$–e_g^{π} orbital splitting energy of ∼1.6 eV in NbO_2 compared to ∼1.3 eV in VO_2; orbital splitting is a key ingredient that stabilizes the cation-dimerized insulating states of both materials. The edge of the O2p-like valence band is estimated to be 3.2 eV below the Fermi level through x-ray photoelectron spectroscopy measurements, suggesting that electrons from O2p states do not contribute to absorption below this energy. This allows us to also assign an observed optical peak at ∼3.0 eV to the Nb $4d_{||} \rightarrow 4d_{||}^*$ transition.

DOI: 10.1103/PhysRevB.90.115135 PACS number(s): 78.20.−e, 79.60.−i, 81.15.−z

I. INTRODUCTON

Temperature-induced metal-insulator transitions (MITs) in oxides are an intriguing problem from both a fundamental materials physics and an applied technology perspective. Since noted in Morin's report of MITs in several binary titanium and vanadium oxides [1], VO_2 has been one of the most studied 3d transition-metal oxides, in part owing to its technologically attractive transition temperature of ∼340 K. Though the precise roles of electron correlations and lattice distortions on the phase transition remain an active area of research, many recent theoretical studies have suggested intimate interplay among the orbital splitting/polarization, correlation effects, and Peierls dimerization of this $3d^1$ system [2–6]. Occupied states have been probed by x-ray photoelectron spectroscopy (XPS) [7], and a rough structure of unoccupied 3d-like states have been deduced by O K-edge x-ray absorption measurements [8–10].

NbO_2 (a $4d^1$ system), like VO_2, crystallizes in a distorted rutile-type structure with Nb dimers and undergoes a temperature-induced MIT, albeit at a considerably higher temperature of ∼1083 K [11]. It is commonly accepted that because 4d orbital valence states are more dispersed in both space and energy, Mott physics is less important in 4d transition-metal oxides than in 3d ones. Along this line of reasoning, it is perhaps surprising that the insulating state of NbO_2 persists to higher temperatures than that of VO_2. A proposed explanation for this difference is that the Peierls effect in NbO_2 is stronger due to larger Nb metal-metal overlap of 4d orbitals, leading to greater orbital splitting between occupied $d_{||}$ states and the unoccupied e_g^{π} states [12]; however, given the many attempts to revise and improve theoretical and computational studies of VO_2 [2–5,13], the physical and electronic properties of NbO_2 also should be examined more thoroughly. If VO_2 and NbO_2 can be compared and contrasted on a similar footing, a better understanding of temperature-induced MITs in d^1 compounds can be attained. Currently, there are few experimental studies that provide insight into the electronic structure of NbO_2.

There have been diffraction [14,15], calorimetry [16], electrical [11,17–19], and magnetic [19] studies on bulk NbO_2, which have shown that it transforms from a high-temperature rutile-structure metal to a low-temperature Nb-dimerized diamagnetic insulator at ∼1083 K. Recently, epitaxial NbO_2 thin films have been grown on (0001) Al_2O_3, (111) MgO, (111) $MgAl_2O_4$, and (111) perovskite oxide substrates [20,21]. The key to achieving (100) epitaxy of rutile-type compounds is exploiting substrate surfaces with eutactic planes [22,23].

In this paper, we study the optical spectra of NbO_2 thin films in their insulating state and compare spectral features to those of VO_2. A combination of valence band XPS and electrical transport measurements are used to assist the interpretation and assignment of peaks in the real optical conductivity spectrum to transitions between electronic states. We deduce a $d_{||}$–e_g^{π} orbital splitting energy of ∼1.6 eV in NbO_2, which is ∼0.3 eV larger than in VO_2. We also deduce the $d_{||} \rightarrow d_{||}^*$ transition to occur at ∼3.0 eV. X-ray photoelectron spectroscopy measurements reveal the positions of the occupied $d_{||}$ and O2p bands with respect to the Fermi level. The separation energies of electronic levels of NbO_2 can be approximated from our experimental data.

II. EXPERIMENTAL

Epitaxial NbO_2 films were grown on (0001) Al_2O_3 by DC reactive sputtering of a Nb metal target at 650 °C, 200 W, 10 mTorr, 7.5 sccm O_2, and 42.5 sccm Ar. An epitaxial (010) VO_2 film was grown on (0001) Al_2O_3 by RF sputtering of a V_2O_5 ceramic target at 450 °C, 150 W, 5 mTorr, 1.3 sccm O_2, and 48.7 sccm Ar. Deposition conditions were optimized to achieve both stoichiometric phases as well as film smoothness for reliable ellipsometry measurements. X-ray reflectivity was used to measure the film thickness, and x-ray diffraction was used for phase and orientation determination. Raman spectroscopy was performed in a confocal microscope using a 532 nm laser source; a filter prevents the collection of signal <170 cm^{-1}. Electrical transport measurements were performed in the van der Pauw geometry; contact pads of 5 nm of Ti and then 50 nm of Au were sputtered on the films. *Ex situ* XPS scans were taken with Al $K\alpha$ radiation and with an electron flood gun that prevents charging; the samples were grounded to the spectrometer. The energy scale of the XPS data is referenced so that the Au4$f_{7/2}$ peak is at 84.0 eV.

Spectroscopic ellipsometry measurements were taken at incident angles of 50° and 70° with respect to the plane

normal. By checking data taken at different in-plane rotations, we confirmed that in-plane anisotropy is not present into our measurements, which is expected because the rutile-type thin films grow with rotational variants and hence threefold in-plane global rotational symmetry [20,22,23]. Furthermore, though our rutile-type films are oriented out of plane, we were able to fit all of our data at both incident angles assuming isotropic optical constants, which may be due to the small path length difference between the p and the s polarized light within the thin films. Thus, our measurements are not sensitive to the possible crystal optical anisotropy of VO_2 and NbO_2. Our optical conductivity spectra should be thought of as polarization averaged. All data sets were fitted both point by point and also separately with analytical oscillators. Point-by-point fitting has the advantage that it does not impose a functional form to the dielectric functions, but analytical oscillator fitting has the advantage that the resultant dielectric functions are ensured to satisfy the Kramers-Kronig relations. Both types of fits for all of our data sets presented here gave quantitatively comparable results. We strove to use the minimum number of oscillators while maintaining high fidelity of fitting so that fitted parameters of different samples can be fairly compared, but the choice of oscillators is not unique. We used a collection of Lorentz and Tauc-Lorentz oscillators; the imaginary part of the dielectric function ε_2 has a functional form with respect to energy E of

$$\varepsilon_2 = \sum_i \frac{A_i B_i^2 E_i E}{\left(E_i^2 - E^2\right)^2 + B_i^2 E^2} + \sum_j \frac{A_j C_j E_j (E - E_{gj})^2}{\left(E^2 - E_j^2\right)^2 + C_j^2 E^2} \frac{\Theta(E - E_{gj})}{E},$$

where Θ is the Heaviside step function. $A_{i(j)}$, B_i, $E_{i(j)}$, E_{gj}, and C_j are the fit parameters for the ith Lorentz oscillator and the jth Tauc-Lorentz oscillator. We will discuss the optical properties of a 38 nm VO_2 (sample V1) as well as 54 and 57 nm NbO_2 films (N1 and N2, respectively).

III. RESULTS

The real optical conductivity $\sigma_1 = \omega\varepsilon_0\varepsilon_2$ of V1, N1, and N2 are shown in Figs. 1(a)–1(c), where ω is the angular photon frequency. Results of the point-by-point and oscillator fits are compared, and the contribution of each individual oscillator is also displayed. Fitted parameters are summarized in Table I. Appendix A includes the raw data taken of N1 as well as the plots of the dielectric functions and optical constants of each sample. The lowest energy optical excitation feature can be fitted adequately mainly by a single Tauc-Lorentz oscillator. The center energy is 1.31 eV for V1 and 1.58 eV for both N1 and N2. Though N1 and N2 should be nominally the same in terms of deposition conditions, aside from a small difference in thickness, we can see that that higher energy (>3.5 eV) features are different; in particular, N2 shows higher conductivity and more spectral features. Nevertheless, their low-energy spectra (<3.5 eV) are quite comparable, as captured by their respective Oscillators 1 and 3 in Table I.

Sum-rule analysis [Fig. 1(d)] can be performed on optical conductivity spectra to determine the effective number of

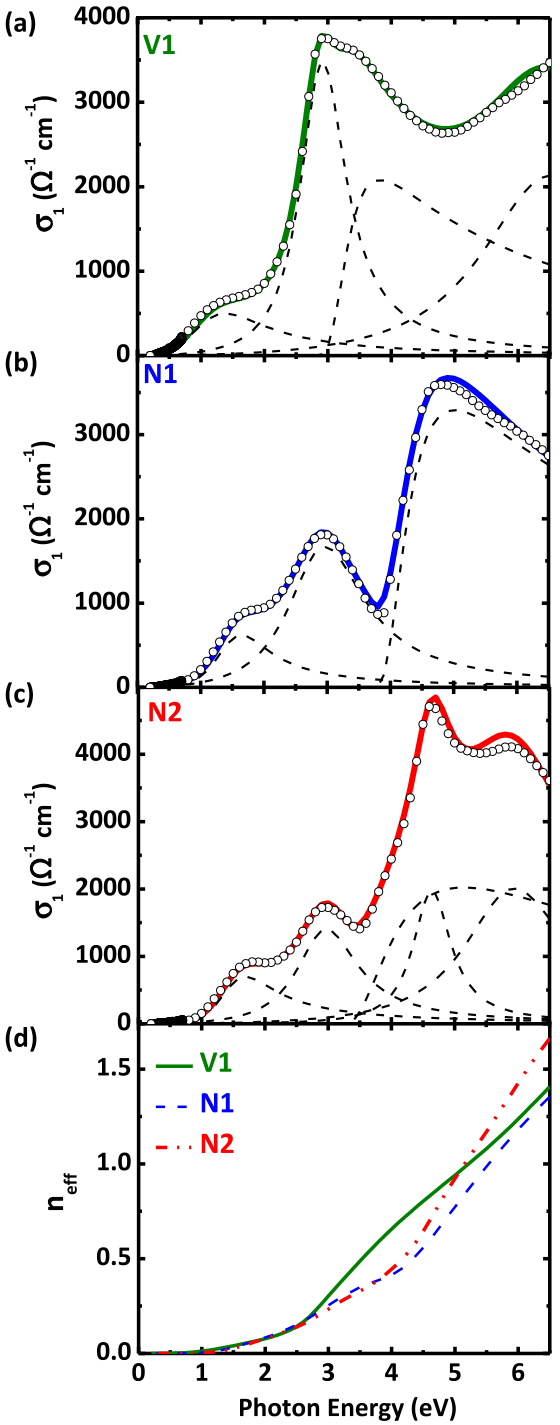

FIG. 1. (Color online) Real optical conductivity σ_1 of (a) V1, (b) N1, and (c) N2, showing the spectra fitted point by point (symbols) as well as by Lorentz and Tauc-Lorentz oscillators (solid lines). The optical conductivity contributions from individual oscillators are shown in the dashed lines. (d) The effective number of electrons n_{eff} involved in optical processes as a function of photon cutoff energy.

electrons n_{eff} per formula unit of NbO_2 accounting for optical excitation from 0 to a cutoff energy of E,

$$n_{\text{eff}}(E) = \frac{2m_0}{N\pi e^2\hbar} \int_0^E \sigma_1(E')dE',$$

TABLE I. Fitted parameters used to calculate the optical conductivity spectra [Figs. 1(a)–1(c)] from spectroscopic ellipsometry. B, C, E, and E_g are in units of electron volts, while A is in units of electron volts for a Tauc-Lorentz oscillator and is dimensionless for a Lorentz oscillator.

	Tauc-Lorentz								Lorentz								
	Oscillator 1				Oscillator 2				Oscillator 3			Oscillator 4			Oscillator 5		
	A_1	E_1	C_1	E_{g1}	A_2	E_2	C_2	E_{g2}	A_3	E_3	B_3	A_4	E_4	B_4	A_5	E_5	B_5
V1	5.78	1.31	1.49	0.19	216	3.13	1.00	2.90	8.93	2.92	0.87	2.43	6.53	2.77			
N1	5.63	1.58	1.06	0.41	449	3.95	1.16	3.79	4.20	2.96	1.47						
N2	9.16	1.58	1.08	0.62	223	3.38	1.86	3.30	3.53	2.97	1.17	3.2	4.64	0.72	2.52	5.95	1.97

where m_0 is the bare electron mass and N is the volume density of formula units of NbO_2 or VO_2.

X-ray diffraction 2θ-θ scans of N1 and N2 reveal that the both of the films are (110)-oriented in using Miller indices of the room-temperature distorted $I4_1/a$ unit cell [15], which corresponds to the pseudorutile (100) orientation [Fig. 2(a)]. The out-of-plane spacings, pseudorutile a lattice parameters, of both samples are 4.835 Å, which is within the range of reported values of bulk crystals [15,24,25]. The film peak of N1 is broader and slightly asymmetric. There is a weak second NbO_2 orientation in N2 but no other peaks for N1. We found slight differences in Raman peak positions, particularly for the mode near 390 cm^{-1}, as well as weaker signal for the mode at 272 cm^{-1} in N1 [Fig. 2(b)]. Moreover, the Raman peaks of N2 are in general more intense and sharper of those of N1. Therefore, the contrast between the optical conductivity of N1 and N2 may be due to minor differences in nonstoichiometric point defect concentrations and/or in residual thin-film strain within the NbO_2 phase. In particular, we believe that N2 is of higher crystalline quality and is likely closer to the exact dioxide stoichiometry compared to N1. While there are Raman measurements on polycrystalline films [26], there have not been experiments on bulk single crystals or phonon spectrum calculations of the low-temperature phase. Note that the apparent differences in the 190 cm^{-1} mode in Fig. 2(b) may arise from an energy filter that blocks signal below ~170 cm^{-1}, resulting in an intensity jump.

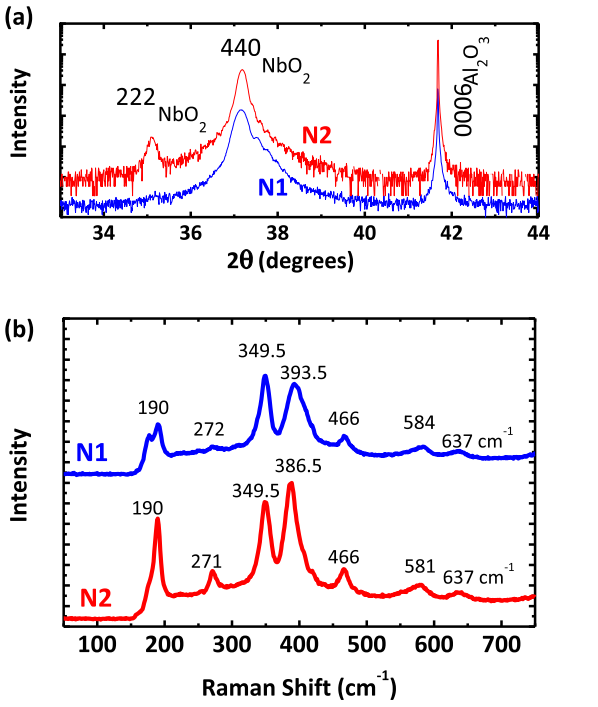

FIG. 2. (Color online) (a) X-ray diffraction 2θ-θ scans and (b) Raman spectra of N1 and N2. The Miller indices used for the NbO_2 peaks refer to its Nb-dimerized tetragonal unit cell. The 440 and 222 reflections correspond to the pseudorutile 200 and 101 reflections, respectively.

X-ray photoelectron spectroscopy was employed to probe the energy positions of the occupied valence band states of V1, N1, and N2 [Fig. 3(a)]. There are two stark differences: (1) emission from occupied valence d electron states is maximized at 0.85 eV for VO_2 and ~1.25 eV for NbO_2 (1.3 eV for N1 and 1.2 eV for N2), and (2) the emission edges of O2p-like states are estimated to be ~2.0 eV for VO_2 and ~3.2 eV for NbO_2. Because the samples are grounded to the spectrometer, the binding energies should be interpreted as the energies with respect to their Fermi levels. Our XPS spectrum of V1 matches closely to that of Shin *et al.* [7]. The O2p band energies of N1 and N2 closely resemble recent *in situ* photoemission studies of epitaxial NbO_2 films grown on (111) perovskite substrates [21]. Since XPS is surface sensitive, and both VO_2 and NbO_2 are susceptible to surface oxidation to their highest oxides, the intensity for transition-metal valence d peak depends on the degree of surface oxidation in ambient conditions. For example, surface oxidation on N1 is more pronounced than on N2. Nevertheless, for seven different NbO_2 films measured, we find that though the relative intensity may differ, the position in energy of Nb4d valence peak does not change to within ±0.1 eV, which is roughly the resolution limit of the XPS system (data not shown). The same is true for the position of the O2p-like band. The higher oxide and NbO_2 differ mainly in 4d electron filling; thus, despite some degree of surface oxidation, the valence band XPS nevertheless yields a good estimate of the O2p band position of NbO_2.

A core-level Nb3d XPS scan of N2 illustrates that there is in fact some unavoidable sample surface oxidation once the sample is exposed to the ambient, showing Nb^{5+} 3d doublets [Fig. 3(b)]. Regardless, there is also a clear signature of Nb^{4+}. Core-level peak positions of N2 are listed in Table II, and they closely match reported values from bulk crystals [27,28]. After background subtraction, the Nb3d core-level XPS spectrum of N2 in Fig. 3(b) was fitted with two doublet pairs. Each pair

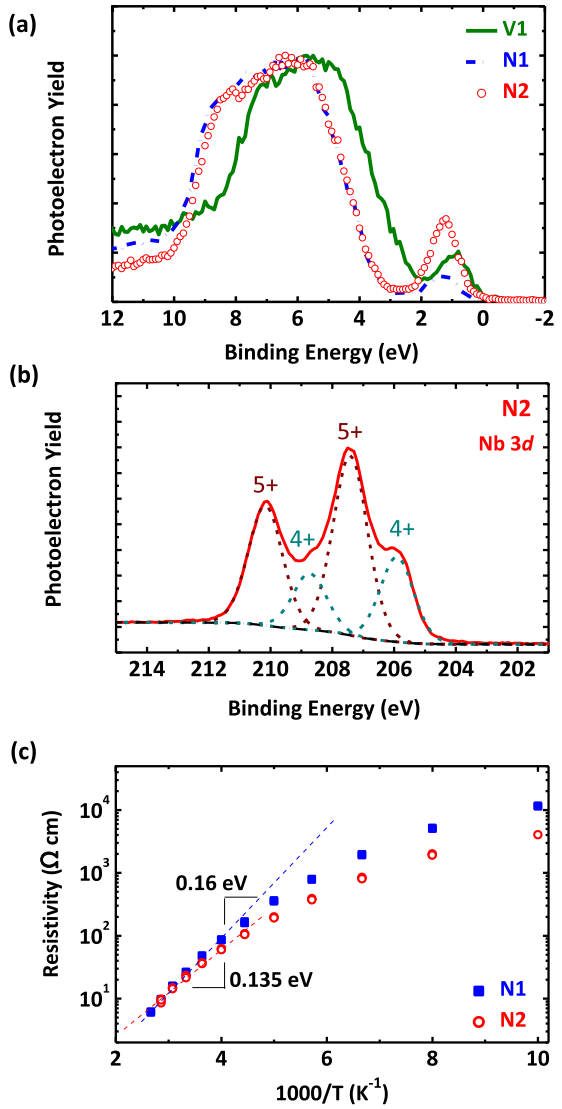

FIG. 3. (Color online) (a) Valence band XPS spectra of V1, N1, and N2; (b) core-level Nb3*d* spectrum of N2; and (c) temperature-dependent electrical transport of N1 and N2.

corresponds to the spin-orbit-split $3d_{5/2}$ and $3d_{3/2}$ levels of two different Nb valence states, 5+ and 4+. For each pair, we constrained the relative integrated intensities between $3d_{5/2}$ and $3d_{3/2}$ to be 3:2 and to possess the same full width at half-maximum (FWHM) values. The FWHM value of fitted Nb^{4+} peaks was 1.28 eV and that of Nb^{5+} was 1.31 eV. The integrated intensity ratio between Nb^{4+} and Nb^{5+} was 31:69. However, we believe that the Nb^{5+} oxide is confined to the very surface because, in our experience, core-level Nb3*d* scans of even elemental Nb metal films show a comparable amount of Nb^{5+} signature due to surface oxidation in ambient conditions. We show in Appendix B that a possible higher oxide at the sample surface does not change the optical features in Fig. 1.

Figure 3(c) reveals the activation energy for electrical conduction to be 0.16 eV for N1 and 0.135 eV for N2. The weaker temperature dependences exhibited by both samples at low temperatures may be indicative of hopping transport via defect states.

TABLE II. Core-level binding energies of N2 in electron volts.

	Nb^{5+}	Nb^{4+}	O
$3d_{5/2}$	207.4	205.9	–
$3d_{3/2}$	210.2	208.7	–
1*s*	–	–	530.6

IV. DISCUSSION

Using Goodenough's nomenclature [29], the antibonding *d*-like states that partake in π bonding with surrounding oxygen are $d_{||}$ and e_g^π (t_{2g} in octahedral symmetry), where $d_{||}$ refers to the orbitals that are also involved in direct metal-metal σ bonding. The two *d*-like orbitals that σ bond with oxygen are referred to as d_σ (e_g in octahedral symmetry). In the dimerized insulating states of both VO_2 and NbO_2, the $d_{||}$ further splits into $d_{||}$ metal bonding and $d_{||}^*$ metal antibonding states. For our discussion, we assume that the arrangement of lowest to highest energy orbitals is $d_{||} \rightarrow e_g^\pi \rightarrow d_{||}^* \rightarrow d_\sigma$, which is supported by a number of computational studies [2,12,30,31]. However, we do acknowledge there should be band overlap, particularly between the e_g^π and $d_{||}^*$ bands. For the purpose of our discussion, we will also assume that the lone *d* electron resides solely in the $d_{||}$ state, but note that computational studies typically do not yield full orbital polarization in the insulating states [2,3,12].

Because the binding energy edge of O2*p*-like states deduced by XPS [Fig. 3(a)] is ~3.2 eV for NbO_2 and ~2.0 eV for VO_2, we assume that excitation of the one 4*d* (3*d*) electron is mainly responsible for the optical conductivity below these energies for NbO_2 (VO_2). This assumption can be justified by the observation that $n_{\rm eff}$ is considerably less than 1 at the stated energies for each compound [Fig. 1(d)]. Table I shows that the center energies of Tauc-Lorentz oscillator used to fit the lowest energy absorption feature are 1.31 eV for V1 and 1.58 eV for N1 and N2. This center energy ranges from 1.56 to 1.67 eV for 10 different NbO_2 thin films measured. In both experimental [32] and theoretical [33] studies of VO_2, similar optical excitation is thought to be indicative of a $d_{||} \rightarrow e_g^\pi$ transition, representative of the essential orbital splitting that is required to stabilize the insulating state. Experimentally, reported peak energies range from 1.1 to 1.35 eV for VO_2 [32,34–37]. Therefore, we assign the peak energy of 1.58 eV in N1 and N2 to be representative of the $d_{||}-e_g^\pi$ orbital splitting; the larger separation in NbO_2 appears to be consistent with its higher transition temperature.

The center energies of Oscillator 1 in N1 and N2 are only slightly larger than the binding-energy peak of the occupied $d_{||}$ band as determined by XPS, which suggests that the Fermi level is close to the conduction band edge and explains the small activation energy observed in electrical transport. Hence, the activation energy should not be interpreted as half of the band gap. In Jannick and Whitmore's [18] electrical transport study of bulk ceramic NbO_2, they found a higher activation energy of ~0.45 eV.

Furthermore, we believe that the center energies of Oscillator 3 in N1 (2.96 eV) and N2 (2.97 eV) are representative of the $d_{||} \rightarrow d_{||}^*$ transition. This assignment is close to the

separation concluded in density functional theory calculations based on the local density approximation, though possible correlation effects were not accounted for [12]. On the other hand, we also note that an older calculation of the joint density of states of NbO_2 performed by Posternak *et al.* [38] does not show a distinct peak at ~3.0 eV. From Jiang and Spence's [39] O K-edge electron energy loss spectroscopy (EELS) studies of NbO_2, they deduced that the octahedral crystal field splitting of *unoccupied* 4d-like π and σ antibonding states to be ~3.5 eV. We assume this value to be the approximate separation between the e_g^{π} and d_{σ} states. Therefore, any possible excitation to the d_{σ} states contributes minimally to that of the peak captured by Oscillator 3. Furthermore, considering the position of the O2p band as deduced by XPS, excitation of electrons from O2p states likewise should contribute insignificantly to the Oscillator 3 peaks of N1 and N2. Table I shows that Oscillator 3 of V1 peaks at 2.92 eV; however, in this sample, the origin is more difficult to isolate because O2$p \rightarrow e_g^{\pi}$ transitions contribute heavily at this energy range, as suggested by previous studies [29,33,36] as well as by the lower O2p photoelectron band edge energy of V1 at 2.0 eV below the Fermi level [Fig. 3(a)]. In VO_2 thin films, Qazilbash *et al.* [32] reported an optical peak at 2.5 eV attributed to the $d_{||} \rightarrow d_{||}^*$ transition, and Verleur *et al.* [36] observed a peak at ~2.75 eV in bulk and ~3.0 eV in thin-film samples but did not assign them to any particular transition. Whether a discernable peak emerges in theoretical optical conductivity calculations of VO_2 depends on the model used and computational details [33].

For NbO_2 at photon energies >3.2 eV, it is clear that a combination of transitions from occupied O2p and $d_{||}$ states are involved, so we do not attempt to make any further assignments of optical features to specific transitions. We must also emphasize that because the choice for oscillators used for the fitting is not unique, though they are useful for the comparison of experimental spectra of different samples, quantitative oscillator strengths (integrated intensity) of *individual* oscillators should not be taken literally. The overall conductivity spectra, however, are quantitative. If excitonic and other excited-state correlation effects can be ignored, Fig. 4 represents a rough schematic of the energy ordering of the different bands (orbitals) with respect to the Fermi level of our NbO_2 samples, as deduced from our optical conductivity and XPS measurements. The position of the d_{σ} states was inferred from Jiang and Spence's [39] O K-edge EELS measurements in addition to our data. Though our experimental results appear consistent with the band calculations of Eyert [12], electron correlations were not included in the theoretical study. A recent *ab initio* study on niobium oxides suggest that a Hubbard U of 2 eV on Nb 4d orbitals may be appropriate [40]. Given that recent work has suggested that correlation effects are sizeable even in 5d transition-metal oxides [41], their contribution in the 4d transition-metal oxide NbO_2 needs to be reexamined.

Last, we can estimate the *optical* gaps of our samples by defining them to be the energy corresponding to $\sigma_1 = 10\,\Omega^{-1}\,\mathrm{cm}^{-1}$ in the point-by-point fit; they are 0.28, 0.34, and 0.36 eV for V1, N1, and N2, respectively. We use the point-by-point results here so that we do not impose a predefined spectral shape of the absorption edge, which would be the case in the oscillator fits.

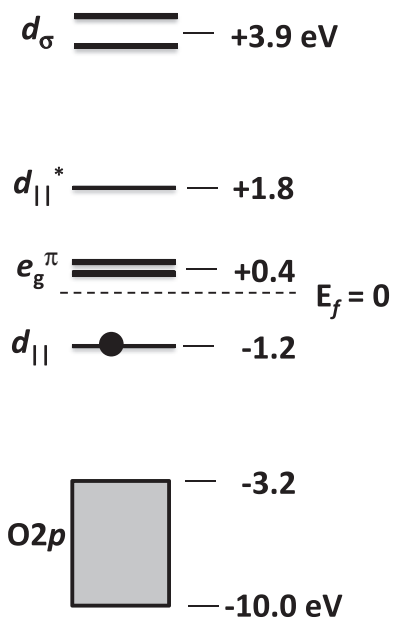

FIG. 4. Proposed, approximate energy arrangement of electron levels of NbO_2 based on the ordering of orbital states suggested by the theoretical study of Ref. [12] along with our measured experimental optical conductivity and valence band XPS features. The position of the d_{σ} states was additionally inferred by an EELS study in Ref. [39].

V. CONCLUSIONS

In conclusion, our study presents the optical conductivity of NbO_2 films with epitaxial variants deposited on (0001) Al_2O_3. XPS measurements indicate that emission from the occupied $d_{||}$ band states peaks at 1.2 eV below the Fermi level, and O2p band edge is ~3.2 eV below the Fermi level. A comparison of the spectral features of NbO_2 and VO_2 states reveals a $d_{||} - e_g^{\pi}$ orbital splitting that is ~0.3 eV larger in NbO_2, which is consistent with its higher MIT temperature. We are able to determine approximate energy separation among Nb 4d-like and O2p-like electronic states based on experimental data. More refined understanding of the spectral properties of NbO_2 would require comparison with new electronic structure calculations that include precise contributions from metal-metal bonding, electronic correlation, and spin-orbit interaction effects.

ACKNOWLEDGMENTS

This work was funded by the National Science Foundation (NSF) and Air Force Office of Scientific Research. The authors acknowledge facility support at the Materials Research Science and Engineering Center Shared Experimental Facilities at the Massachusetts Institute of Technology, supported by the NSF under Award No. DMR-08-19762 as well as at the Center for Nanoscale Systems (CNS), a member of the National Nanotechnology Infrastructure Network (NNIN) at Harvard University, supported by the NSF under NSF Award No. ECS-0335765. F. J. Wong thanks J. Tresbeck of CNS for technical assistance on electrical transport measurements, and N. Hong thanks T. Tiwald of J. A. Woollam Co. for

useful discussions and comments on far infrared ellipsometry measurements.

APPENDIX A: ELLIPSOMETRY—FITTING PROTOCOL

Ellipsometry data Ψ and Δ are taken from 0.2 to 6.5 eV at incident angles of 50° and 70° with respect to the surface normal; the raw data of N1 are shown in Fig. 5. An optical model consisting of a 0.5 mm of Al_2O_3 substrate layer with known optical constants (refractive index n and attenuation index k) and a 54 nm film layer with unknown optical constants, to be determined, was created [42]. Since the film thickness was measured independently by x-ray reflectivity, it was not treated as a fit parameter. Each data set was fitted by two methods: (1) the n and k values at each energy of the 54 nm film layer were fitted point-by-point to reproduce the corresponding observed Ψ and Δ values, and (2) a series of Kramers-Kronig-consistent oscillators with analytical dielectric functions and adjustable parameters were used to fit to the Ψ and Δ spectra. Figure 5 also includes the Ψ and Δ values generated by the oscillator model of N1, showing a good match across the entire spectrum of energies. The optical anisotropy of Al_2O_3 is minimal [43], and an isotropic approximation is valid within the measured spectral range [44]. We also assumed that dielectric function of the film layer to be isotropic. Because both the 50° and 70° can be fitted to high accuracy simultaneously with the assumption of an optically isotropic film, we believe that we our fits are in fact representative of the optical response of our NbO_2 films with epitaxial variants [20]. We checked data taken at incident angles of 60°, 65°, and 75° as well and found that the different incident angles yielded quantitatively similar fits. Analogous results from the point-by-point fits result in comparably high-fidelity matching of observed and modeled Ψ and Δ values (fits not shown). The accuracy of fitting by both the point-by-point and oscillator methods is typical of all

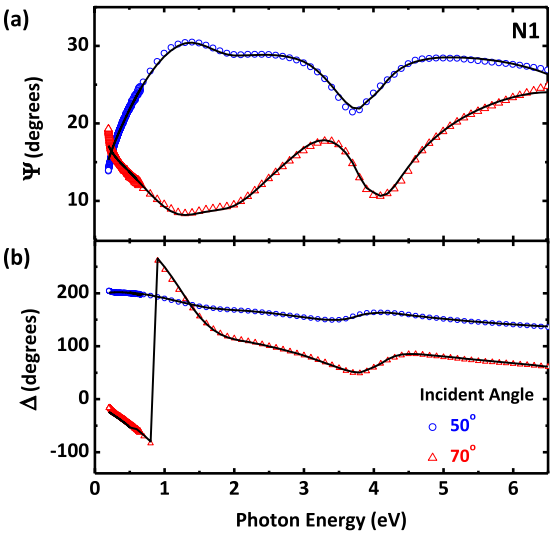

FIG. 5. (Color online) Ellipsometry data (a) Ψ and (b) Δ of N1 taken at two different incident angles. The raw data are shown as open symbols, and fits derived from an oscillator model are shown as lines.

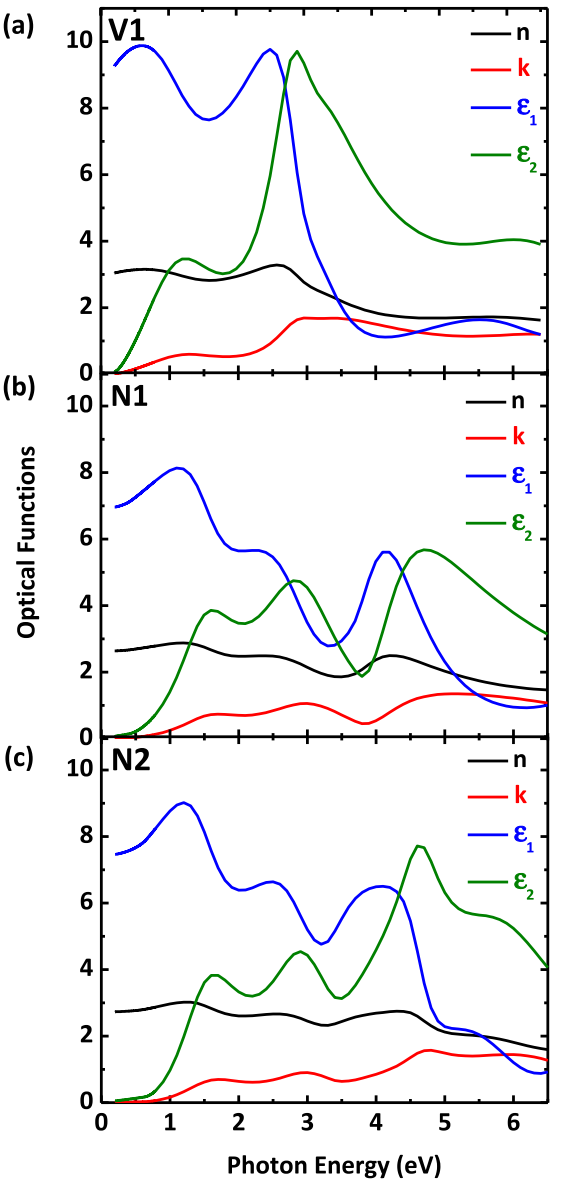

FIG. 6. (Color online) The spectra of n, k, ε_1, and ε_2 of (a) V1, (b) N1, and (c) N2 attained by oscillator fits.

three samples in the study. The n, k, ε_1, and ε_2 spectra of V1, N1, and N2 are shown in Fig. 6.

APPENDIX B: EILIPSOMETRY—EFFECT OF POSSIBLE HIGHER SURFACE OXIDE

It is possible that the surfaces of films transform to the highest stoichiometric oxides, as is suggested by Fig. 3(b). To test how a possible surface layer of Nb_2O_5 would affect our optical conductivity spectra, we formed a model sample of 0.5 mm Al_2O_3, 52 nm film with unknown optical constants and a 2 nm surface layer of Nb_2O_5 with known optical constants [Fig. 7(b)] to perform a point-by-point fit to the ellipsometry data of N1 (note that we kept the total film thickness to be 54 nm). Results of a point-by-point fit of the optical conductivity with and without a surface Nb_2O_5 layer are shown in Fig. 7(a). Since from x-ray reflectivity

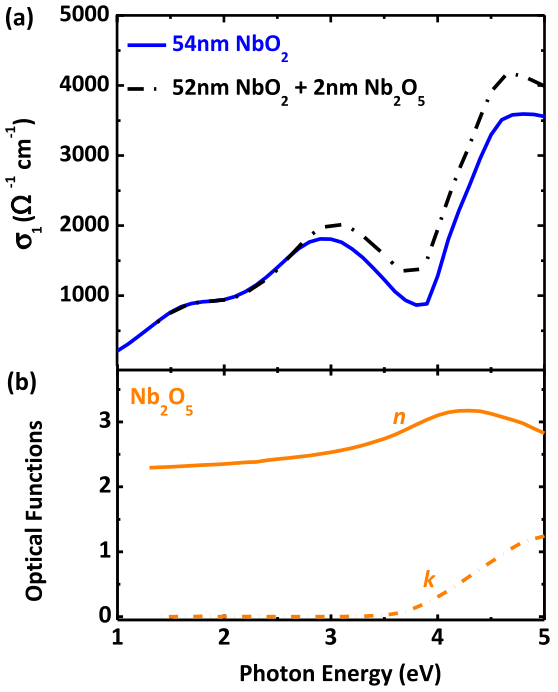

FIG. 7. (Color online) (a) The optical conductivity of N1 modeled as a homogenous 54 nm film versus a 52 nm film with an additional 2 nm Nb_2O_5 surface layer attained by point-by-point fits. (b) The optical constants of Nb_2O_5 used in the fitting of (a).

there is no readily detectable surface layer with different x-ray scattering contrast, we believe that a hypothetical 2-nm-thick Nb_2O_5 layer represents the maximum thickness. The optical conductivity values are somewhat different when Nb_2O_5 becomes absorbing (>3 eV) but maintains the same overall spectral shape, and there is no discernable difference for photon energies <2.5 eV. Therefore, a higher surface oxide will not change the main optical features and would only affect the exact conductivity values at higher photon energies.

TABLE III. The 1*s* XPS peak positions in electron volts of adventitious carbon and oxygen of V1, N1, V2, as well as the Au and Ag references. Several different Au samples were measured, and the range of C1*s* peak positions is listed.

Sample	C1*s*	O1*s*
Au	284.0–284.4	–
Ag	285.2	–
V1	284.6	529.7
N1	285.3	530.7
N2	285.4	530.6

APPENDIX C: XPS—ENERGY REFERENCE

The Au4$f_{7/2}$ peak was measured at 84.08 eV, and the Ag3$d_{5/2}$ peak was measured at 368.38 eV; therefore, the measured spectra were shifted by −0.08 eV such that Au4$f_{7/2}$ and Ag3$d_{5/2}$ occur at 84.0 and 368.3 eV, respectively, which are standard reference values [45].

We did not perform any other shifting of our measured spectra based on adventitious carbon for three reasons. First, we used an electron flood gun, which neutralizes the samples during measurement; therefore, sample charging is not expected to be an issue. Second, the resistivity of NbO_2 films are on the order of 20 Ω cm and VO_2 is about 1 Ω cm at room temperature, both of which are still reasonably conductive. It has been our experience that Ohmic contacts can readily be established on both films, and they can be properly grounded to the sample holder and hence the spectrometer. Last, we have found that the adventitious C1*s* peaks vary depending on underlying material. Table III shows that the C1*s* binding energies differ by ∼1.0 eV between the Au and Ag reference samples when sample charging is certainly not an issue. For completeness as well as reference purposes, Table III lists the C1*s* as well as the O1*s* peak positions of V1, N1, and N2.

[1] F. J. Morin, Phys. Rev. Lett. **3**, 34 (1959).
[2] S. Biermann, A. Poteryaev, A. I. Lichtenstein, and A. Georges, Phys. Rev. Lett. **94**, 026404 (2005).
[3] X. Yuan, Y. B. Zhang, T. A. Abtew, P. H. Zhang, and W. Q. Zhang, Phys. Rev. B **86**, 235103 (2012).
[4] C. Weber, D. D. O'Regan, N. D. M. Hine, M. C. Payne, G. Kotliar, and P. B. Littlewood, Phys. Rev. Lett. **108**, 256402 (2012).
[5] Z. Y. Zhu and U. Schwingenschlogl, Phys. Rev. B **86**, 075149 (2012).
[6] M. W. Haverkort, Z. Hu, A. Tanaka, W. Reichelt, S. V. Streltsov, M. A. Korotin, V. I. Anisimov, H. H. Hsieh, H. J. Lin, C. T. Chen, D. I. Khomskii, and L. H. Tjeng, Phys. Rev. Lett. **95**, 196404 (2005).
[7] S. Shin, S. Suga, M. Taniguchi, M. Fujisawa, H. Kanzaki, A. Fujimori, H. Daimon, Y. Ueda, K. Kosuge, and S. Kachi, Phys. Rev. B **41**, 4993 (1990).
[8] T. C. Koethe, Z. Hu, M. W. Haverkort, C. Schussler-Langeheine, F. Venturini, N. B. Brookes, O. Tjernberg, W. Reichelt, H. H. Hsieh, H. J. Lin, C. T. Chen, and L. H. Tjeng, Phys. Rev. Lett. **97**, 116402 (2006).
[9] J. Laverock, A. R. H. Preston, D. Newby, K. E. Smith, S. Sallis, L. F. J. Piper, S. Kittiwatanakul, J. W. Lu, S. A. Wolf, M. Leandersson, and T. Balasubramanian, Phys. Rev. B **86**, 195124 (2012).
[10] D. Ruzmetov, S. D. Senanayake, V. Narayanamurti, and S. Ramanathan, Phys. Rev. B **77**, 195442 (2008).
[11] Y. Sakai, N. Tsuda, and T. Sakata, J. Phys. Soc. Jpn. **54**, 1514 (1985).
[12] V. Eyert, Europhys. Lett. **58**, 851 (2002).
[13] V. Eyert, Phys. Rev. Lett. **107**, 016401 (2011).
[14] S. M. Shapiro, J. D. Axe, G. Shirane, and P. M. Raccah, Solid State Commun. **15**, 377 (1974).
[15] A. A. Bolzan, C. Fong, B. J. Kennedy, and C. J. Howard, J. Solid State Chem. **113**, 9 (1994).
[16] K. Seta and K. Naito, J. Chem. Thermodyn. **14**, 921 (1982).
[17] T. Sakata, K. Sakata, and I. Nishida, Physica Status Solidi **20**, K155 (1967).

[18] R. F. Janninck and D. H. Whitmore, J. Phys. Chem. Solids **27**, 1183 (1966).
[19] K. Sakata, J. Phys. Soc. Jpn. **26**, 867 (1969).
[20] F. J. Wong and S. Ramanathan, J. Mater. Res. **28**, 2555 (2013).
[21] A. B. Posadas, A. O'Hara, S. Rangan, R. A. Bartynski, and A. A. Demkov, Appl. Phys. Lett. **104**, 092901 (2014).
[22] F. J. Wong, Y. Zhou, and S. Ramanathan, J. Cryst. Growth **364**, 74 (2013).
[23] F. J. Wong and S. Ramanathan, J. Vac. Sci. Technol. A **32**, 040801 (2014).
[24] R. Pynn, J. D. Axe, and R. Thomas, Phys. Rev. B **13**, 2965 (1976).
[25] A. K. Cheetham and C. N. R. Rao, Acta Crystallogr. B **32**, 1579 (1976).
[26] Y. Zhao, Z. J. Zhang, and Y. H. Lin, J. Phys. D Appl. Phys. **37**, 3392 (2004).
[27] M. K. Bahl, J. Phys. Chem. Solids **36**, 485 (1975).
[28] R. Fontaine, R. Caillat, L. Feve, and M. J. Guittet, J. Electron Spectrosc. **10**, 349 (1977).
[29] J. B. Goodenough, J. Solid State Chem. **3**, 490 (1971).
[30] V. Eyert, Ann. Phys. (Berlin) **11**, 650 (2002).
[31] J. M. Tomczak and S. Biermann, J. Phys.: Condens. Matter **19**, 365206 (2007).
[32] M. M. Qazilbash, A. A. Schafgans, K. S. Burch, S. J. Yun, B. G. Chae, B. J. Kim, H. T. Kim, and D. N. Basov, Phys. Rev. B **77**, 115121 (2008).
[33] J. M. Tomczak and S. Biermann, Phys. Rev. B **80**, 085117 (2009).
[34] K. Okazaki, S. Sugai, Y. Muraoka, and Z. Hiroi, Phys. Rev. B **73**, 165116 (2006).
[35] M. Nazari, Y. Zhao, V. V. Kuryatkov, Z. Y. Fan, A. A. Bernussi, and M. Holtz, Phys. Rev. B **87**, 035142 (2013).
[36] H. W. Verleur, A. S. Barker, and C. N. Berglund, Phys. Rev. **172**, 788 (1968).
[37] W. W. Li, Q. Yu, J. R. Liang, K. Jiang, Z. G. Hu, J. Liu, H. D. Chen, and J. H. Chu, Appl. Phys. Lett. **99**, 241903 (2011).
[38] M. Posternak, A. J. Freeman, and D. E. Ellis, Phys. Rev. B **19**, 6555 (1979).
[39] N. Jiang and J. C. H. Spence, Phys. Rev. B **70**, 245117 (2004).
[40] W. B. Zhang, W. D. Wu, X. M. Wang, X. L. Cheng, D. W. Yan, C. L. Shen, L. P. Peng, Y. Y. Wang, and L. Bai, Surf. Interface Anal. **45**, 1206 (2013).
[41] M. M. Sala, K. Ohgushi, A. Al-Zein, Y. Hirata, G. Monaco, and M. Krisch, Phys. Rev. Lett. **112**, 176402 (2014).
[42] J. A. Woollam, B. Johs, C. M. Herzinger, J. Hilfiker, R. Synowicki, and C. L. Bungay, Crit. Rev. Op. **CR72**, 3 (1999).
[43] F. Gervais, in *Handbook of Optical Constants of Solid II*, edited by E. D. Palik (Academic Press, San Diego, 1991), p. 761.
[44] D. E. Aspnes, J. Opt. Soc. Am. **70**, 1275 (1980).
[45] M. P. Seah, L. S. Gilmore, and G. Beamson, Surf. Interface Anal. **26**, 642 (1998).